Theoretical Study on the Mechanism of the ^{1}CHF + NO Reaction

Jian-jun Liu, Yi-hong Ding, Ji-kang Feng,* and Chia-chung Sun

State Key Laboratory of Theoretical and Computational Chemistry, Jilin University, Changchun, Jilin 130023, P. R. China

Received: April 24, 2001; In Final Form: August 27, 2001

The complex doublet potential energy surface of the CHFNO system is investigated at the QCISD(T)/6-311G(df,p)//B3LYP/6-311G(d,p) level in order to explore the possible reaction mechanism of ^{1}CHF radical with NO. Twenty-six minimum isomers and fifty-nine transition states are located. Various possible reaction pathways are probed. It is shown that five dissociation products **P$_1$** HF + NCO, **P$_2$** F + HNCO, **P$_4$** OH + FCN, **P$_5$** F + HOCN, and **P$_7$** ^{3}NH + FCO are both thermodynamically and kinetically accessible. Among the five dissociation products, **P$_2$** and **P$_4$** may be the most abundant products with comparable quantities, whereas **P$_1$** is much less competitive followed by the almost negligible **P$_5$** and **P$_7$**. Our results are in marked difference from previous experimental observation that only two dissociation products **P$_1$** and **P$_2$** are identified with the branching ratio being 6:4. However, and despite some energetic differences, our calculated potential energy surface features are quite in parallel to those of the analogous reaction ^{3}CH$_2$ + NO that has been extensively studied. Therefore, future experimental reinvestigations are desirable to clarify the mechanism of the title reaction. The present study may be useful for understanding the CHF chemistry.

1. Introduction

The halogenated carbenes are important intermediates in the incineration of fluorine- and chlorine-containing wastes and in the combustion inhibition mechanisms of fluorine-, bromine-, and iodine-containing flame suppressants.[1] A large number of experimental investigations have been carried out on the CHF reactions.[2−7] Among them, the title reaction CHF + NO may be of particular interest due to its simplicity and the importance of the reactant nitric oxide (NO), which can be formed by the direct or indirect oxidation of atmospheric nitrogen.[8] The title reaction may thus be considered a process referred to as "reburning"[9−12] and may play an important role in decreasing the amount of NO emitted. Obviously, the studies of the key reaction products of ^{1}CHF with NO are very valuable to atmospheric chemistry.

There have been two experimental studies concerning the title reaction. In 1982, Hancock et al.[13] measured the removal rate of CHF in the singlet ground electronic state to be $(7.0 \pm 0.4) \times 10^{-12}$ cm^3 molecule^{-1} s^{-1} at 295 K. In this report, only the channel **P$_1$** HF + NCO was identified. In their later study[14] in 1996, they observed the products NCO, HF, and F by time-resolved Fourier transform infrared (FTIR) emission spectroscopy (F atoms were detected by DF though D_2 addition). As a result, they suggested that a second channel forming F atoms is also significant, i.e., **P$_2$** F + HNCO. They assigned a branching ratio of 0.6 ± 0.04 and 0.4 ± 0.03 to **P$_1$** and **P$_2$**, respectively.

To our best knowledge, there is no theoretical study on the title reaction up to now. Simply from the thermodynamic data,[15−17] this reaction may have other exothermic channels such as **P$_3$** CO + NFH (−41.6 kcal/mol), **P$_4$** OH + FCN (−33.5 kcal/mol), **P$_5$** F + HOCN (−39.0 kcal/mol), and **P$_7$** ^{3}NH + FCO (−14.8 kcal/mol) in addition to the experimentally observed **P$_1$** HF + NCO (−86.0 kcal/mol) and **P$_2$** F + HNCO (−64.1 kcal/mol). On the other hand, the analogous reaction CH_2 + NO has been extensively studied.[16−25] Note that CH_2 is in the triplet ground electronic state. H + HCNO (84%) and OH + HCN (15%) were found to be the almost exclusive products by experiments.[16] Yet, recent extensive theoretical investigations by Shapley et al.[24,25] reveal sharp discrepancies concerning the final product distribution; i.e., they predicted that the products H + HNCO, H + HOCN, and NH_2 + CO should also have comparable yields to OH + HCN. Clearly, the observed product distributions for the reactions of ^{1}CHF and ^{3}CH$_2$ with NO are quite different. A detailed theoretical study on the potential energy surface of ^{1}CHF + NO is then very desirable to disclose why the low-lying products **P$_3$**, **P$_4$**, **P$_5$**, and **P$_7$** were not observed in experiments and to make a mechanistic comparison with the analogous ^{3}CH$_2$ + NO reaction. Such a theoretical study is reported in this paper.

2. Computational Methods

All calculations are carried out using the Gaussian 98 program.[26] The geometries of all the reactants, products, various intermediates, and transition states for the ^{1}CHF + NO reaction are optimized using hybrid density functional B3LYP method with the 6-311G(d,p) basis set. Vibrational frequencies are calculated at the B3LYP/6-311G(d,p) level to check whether the obtained stationary points correspond to isomers or to first-order transition states. To confirm that the transition state connects designated intermediates, we also perform intrinsic reaction coordinate (IRC) calculations at the B3LYP/6-311G-(d,p) level. In addition, single point energies are calculated for the B3LYP/6-311G(d,p) optimized geometries with the quadratic configuration interaction method with single and double excitation and perturbative corrections for triple excitations (QCISD-(T)) with the 6-311G(df,p) basis set. Unless otherwise specified, the QCISD(T) single-point energies are used in the following discussions. For the present doublet system CHFNO, the spin contamination is not severe; i.e., the $\langle S^2 \rangle$ value of each isomer is less than 0.76, very close to the expected value of the pure doublet state 0.75.

10.1021/jp011547i CCC: $20.00
Published on Web 10/10/2001

TABLE 1: Zero-Point Vibration Energies (hartree), Total Energies (TE) (hartree), and Relative Energies (RE) (kcal/mol) for Reactants and Products at the B3LYP/6-311G(d,p) Level and the QCISD(T)/6-311G(df,p)//B3LYP/6-311G(d,p) Level

species	ZPE	BTE	BRE	QTE	QRE	exp
R ^{1}CHF + NO	0.016842	−268.371981	0.0	−267.866857	0.0	
$\mathbf{P_1}$ HF + NCO	0.019393	−268.519730	−91.1	−268.006363	−85.9	−86.6
$\mathbf{P_2}$ F + HNCO	0.021343	−268.486780	−69.2	−267.973825	−64.3	−64.1
$\mathbf{P_3}$ CO + NFH	0.018256	−268.456529	−52.2	−267.949656	−51.1	−41.6
$\mathbf{P_4}$ OH + FCN	0.018627	−268.444649	−44.5	−267.938216	−43.7	−33.7
$\mathbf{P_5}$ F + HOCN	0.021579	−268.441294	−40.5	−267.934859	−39.7	−39.0
$\mathbf{P_6}$ HF + CNO	0.018208	−268.418990	−28.6	−267.904879	−23.0	
$\mathbf{P_7}$ ^{3}NH + FCO	0.015660	−268.398644	−17.5	−267.891179	−16.1	−14.8
$\mathbf{P_8}$ HF + c-CNO	0.016197	−268.386244	−9.4	−267.883297	−10.7	
$\mathbf{P_9}$ H + FNCO	0.013510	−268.391183	−11.4	−267.879522	−10.0	
$\mathbf{P_{10}}$ H + c-C(F)NO	0.013165	−268.358878	5.9	−267.861050	1.3	
$\mathbf{P_{11}}$ FO + HCN	0.018970	−268.376117	9.3	−267.860393	5.4	
$\mathbf{P_{12}}$ F + HCNO	0.019350	−268.376416	−1.2	−267.860483	5.5	7.2
$\mathbf{P_{13}}$ ^{3}NF + HCO	0.015551	−268.369119	1.0	−267.854920	6.7	1.0
$\mathbf{P_{14}}$ H + FCNO	0.013392	−268.344258	15.2	−267.837074	16.5	
$\mathbf{P_{15}}$ F + CNOH	0.020240	−268.346531	18.1	−267.840574	18.6	
$\mathbf{P_{16}}$ F + c−C(H)NO	0.019893	−268.338826	22.7	−267.836850	20.7	
$\mathbf{P_{17}}$ ^{2}CF + HNO	0.016787	−268.328603	27.2	−267.823551	27.1	
$\mathbf{P_{18}}$ ^{2}CF + HON	0.016649	−268.296549	47.2	−267.789831	48.2	

3. Results and Discussions

3.1. Isomers and Products. Starting from the reactant **R** ^{1}CHF + NO, eighteen products are considered, including $\mathbf{P_1}$ HF + NCO (−85.9), $\mathbf{P_2}$ F + HNCO (−64.3), $\mathbf{P_3}$ CO + NFH (−51.1), $\mathbf{P_4}$ OH + FCN (−43.7), $\mathbf{P_5}$ F + HOCN (−39.7), $\mathbf{P_6}$ HF + CNO (−23.0), $\mathbf{P_7}$ 3NH + FCN (−16.1), $\mathbf{P_8}$ HF + c-CNO (−10.7), $\mathbf{P_9}$ H + FNCO (−10.0), $\mathbf{P_{10}}$ H + c-C(F)NO (1.3), $\mathbf{P_{11}}$ FO + HCN (5.4), $\mathbf{P_{12}}$ F + HCNO (5.5), $\mathbf{P_{13}}$ ^{3}NF + HCO (6.7), $\mathbf{P_{14}}$ H + FCNO (16.5), $\mathbf{P_{15}}$ F + HONC (18.6), $\mathbf{P_{16}}$ F + H-c-CNO (20.7), $\mathbf{P_{17}}$ CF + HNO (27.1), and $\mathbf{P_{18}}$ CF + HON (48.2). These products are numbered according to their relative energies with reference to the reactant **R** ^{1}CHF + NO, as listed in Table 1. Simply from the relative energies, we can conclude that the former nine products $\mathbf{P_1}$−$\mathbf{P_9}$ all lie below the reactant **R**. Thus, they are at least thermodynamically feasible. The remaining nine products $\mathbf{P_{10}}$−$\mathbf{P_{18}}$ are surely not feasible due to their high energy, and they are not considered in later mechanistic discussions.

It is worthwhile to compare our calculated relative energies with the experimentally determined reaction heats of various products.[22,27,28] As shown in Table 1, for most products, the theoretical and experimental values agree very well, except for $\mathbf{P_3}$ CO + NFH and $\mathbf{P_4}$ OH + FCN with considerable discrepancies 9.5 and 10.0 kcal/mol, respectively.

In view of the diversity of the final products, complex rearrangement may take place via various stable or unstable intermediates. For the present ^{1}CHF + NO reaction, twenty-two open-chain isomers, three cyclic isomers and one weakly bound complex are obtained and their structures are shown in Figure 1. Their energetic data are listed in Table 2. According to the frame structures, the 22 open-chain isomers can be divided into three groups, i.e., species with CNO, NCO and CON skeletons, which are named **a**, **b**, **c**, respectively. The three cyclic isomers ($\mathbf{d_1}$, $\mathbf{d_2}$, $\mathbf{d_2'}$) are important intermediates between the chain isomers.

As shown in Table 2, the NCO-chain isomer HNC(F)O $\mathbf{b_1}$ lies 96.6 kcal/mol below the reactant **R**, and $\mathbf{b_1}$ is the lowest energy of all isomers. The following low-lying isomers are *cis*-NC(F)OH ($\mathbf{b_2}$) (−86.4), *trans*-NC(F)OH ($\mathbf{b_2'}$) (−84.2), *cis*-FNC(H)O ($\mathbf{b_3}$) (−63.4), and *trans*-FNC(H)O ($\mathbf{b_3'}$) (−62.4) with the relative energies in kcal/mol in parentheses. Generally, the energetic stability order of the three kinds of open-chain isomers are **b** > **a** > **c**.

3.2. Isomerization and Dissociation. To ascertain the interrelation between various HFCNO isomers and dissociation products, fifty-nine transition states are located, which are denoted as the symbols "**TSxy**". For example, $\mathbf{TSa_1d_1}$ denotes the transition state connecting the isomers $\mathbf{a_1}$ and $\mathbf{d_1}$. The optimized structures of the transition states are shown in Figure 2, and their energies are listed in Table 3. By means of the isomers, products, transition states and the corresponding energies, the schematic profiles of the potential energy surface are depicted in Figure 3 and Figure 4.

TABLE 2: Zero-Point Vibration Energies (hartree), Total Energies (TE) (hartree), and Relative Energies (RE) (kcal/mol) for All Isomers at the B3LYP/6-311G(d,p) Level and the QCISD(T)/6-311G(df,p)//B3LYP/6-311G(d,p) Level

species	ZPE	BTE	BRE	QTE	QRE
$\mathbf{a_1}$	0.024446	−268.483936	−65.5	−267.964383	−56.4
$\mathbf{a_1'}$	0.024948	−268.486374	−66.7	−267.966725	−57.6
$\mathbf{a_2}$	0.024039	−268.428200	−30.8	−267.912650	−24.2
$\mathbf{a_2'}$	0.023688	−268.428752	−31.3	−267.912559	−24.4
$\mathbf{a_3}$	0.023942	−268.438698	−37.4	−267.926203	32.8
$\mathbf{a_3'}$	0.024376	−268.443910	−40.4	−267.931475	−35.8
$\mathbf{a_3''}$	0.024331	−268.437973	−36.7	−267.924616	−31.5
$\mathbf{a_3'''}$	0.023875	−268.430265	−32.2	−267.916968	−27.0
$\mathbf{b_1}$	0.024011	−268.540289	−101.1	−268.027897	−96.6
$\mathbf{b_2}$	0.025452	−268.522838	−89.3	−268.013213	−86.4
$\mathbf{b_2'}$	0.024804	−268.519197	−87.4	−268.008955	−84.2
$\mathbf{b_3}$	0.023369	−268.467189	−55.7	−267.951051	−63.4
$\mathbf{b_3'}$	0.023645	−268.465012	−54.1	−267.949300	−62.3
$\mathbf{b_4}$	0.023641	−268.435049	−35.3	−267.918232	−42.8
$\mathbf{b_4'}$	0.023084	−268.433979	−35.0	−267.917347	−42.3
$\mathbf{b_5}$	0.024157	−268.463998	−53.2	−267.945469	−44.7
$\mathbf{c_1}$	0.022065	−268.396141	−11.9	−267.878686	−4.1
$\mathbf{c_1'}$	0.022511	−268.399562	−13.8	−267.881879	−5.9
$\mathbf{c_2}$	0.022546	−268.409022	−19.7	−267.900985	−17.8
$\mathbf{c_2'}$	0.022449	−268.408007	−19.1	−267.900203	−17.4
$\mathbf{c_2''}$	0.021974	−268.406808	−18.6	−267.897676	−16.1
$\mathbf{c_2'''}$	0.021648	−268.403126	−16.5	−267.893077	−13.5
$\mathbf{d_1}$	0.024949	−268.466833	−54.4	−267.961832	−54.5
$\mathbf{d_2}$	0.024963	−268.426659	−29.2	−267.921704	−29.3
$\mathbf{d_2'}$	0.024719	−268.424933	−28.3	−267.919550	−28.1
F...HNCO	0.022714	−268.504323	−79.4	−267.974215	−63.7

The attack of the singlet CHF at the doublet NO radical may have three possible ways, i.e., O-end attack, N-end attack, or NO-π-bond attack. There are substantial barriers 14.0 and 8.0 kcal/mol for the O-attack to form the CON-chain isomers HFCON $\mathbf{c_1}$ and $\mathbf{c_1'}$, respectively. This clearly excludes the feasibility of the O-attack. At the B3LYP/6-311G(d,p) level, we are not able to locate any addition transition states from **R** to the CNO-chain isomers HFCNO $\mathbf{a_1}$ and $\mathbf{a_1'}$, as shown by the

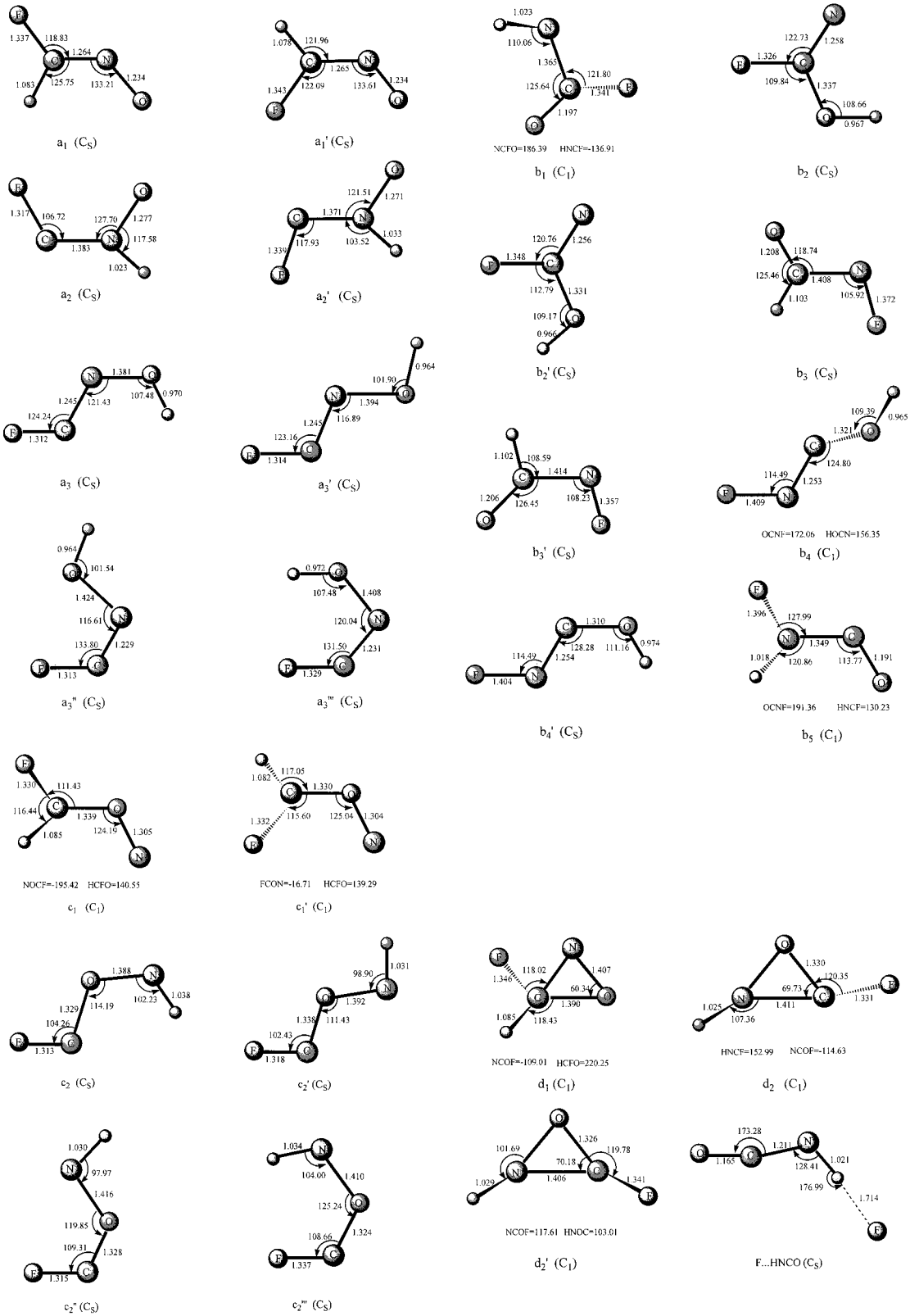

Figure 1. B3LYP/6-311G(d,p)-optimized geometries of all isomers. Bond distances are in angstroms and angles are in degrees.

calculated dissociation curves of $\mathbf{a_1}$ and $\mathbf{a_1'}$ as plotted in Figure 5a,b. Interestingly, at the HF/6-311G(d,p) level, the addition transition states $\mathbf{TSRa_1}$ and $\mathbf{TSRa_1'}$ can be located, as shown in Figure 2. However, the single-point QCISD(T)/6-311G(df,p)//HF/6-311G(d,p) calculations with ZPE correction show that $\mathbf{TSRa_1}$ and $\mathbf{TSRa_1'}$ are −5.6 and −6.3 kcal/mol, respectively, lower than **R** ^{1}CHF + NO. Further QCISD/6-311G(d,p) optimization of the two entrance transition states often leads to the separate fragments CHF and NO. Therefore, we expect that the title reaction may possess a very small or even zero barrier height to form $\mathbf{a_1}$ and $\mathbf{a_1'}$. As will be shown in section 3.3, an entrance barrier height of 0.2 kcal/mol may be consistent with the experimentally measured rate constant. We notice that for the analogous reaction $^3CH_2$ + NO, it was predicted that no entrance barrier would exist to form the N-attack chainlike isomer H_2CNO, whereas a substantial barrier (about 8 kcal/

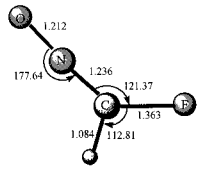

TSa_1a_1' (c_s)

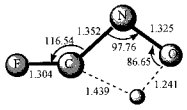

TSa_1a_3 (C_S)

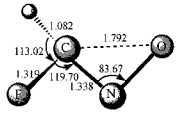

FCNO=-125.00 HCNO=-57.83

TSa_1d_1 (C_1)

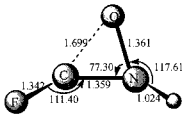

ONCF=-101.09 HNOC=235.04

$TSa_2'd_2'$ (C_1)

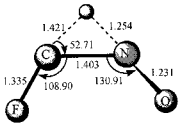

ONCF=-4.89 HCNF=247.15

$TSa_1'a_2$ (C_1)

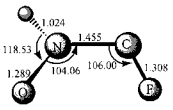

FCNO=103.05 HNOC=219.96

TSa_2a_2' (C_1)

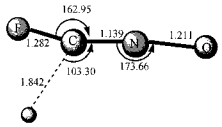

TSa_1P_{14} (C_S)

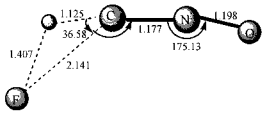

$TSa_1'P_6$ (C_S)

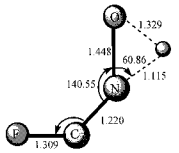

TSa_2a_3'' (C_S)

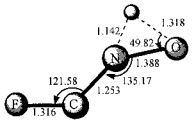

$TSa_2'a_3'$ (C_S)

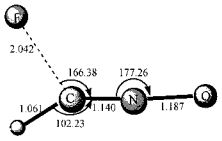

$TSa_1'P_{12}$ (C_S)

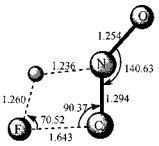

$TSa_2'P_6$ (C_S)

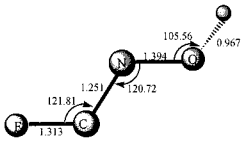

HONC=70.16

TSa_3a_3'

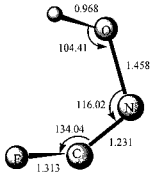

ONCF=-2.03 HONC=67.99

$TSa_3''a_3'''$ (C_1)

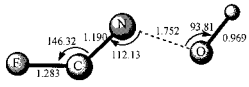

$TSa_3'P_4$ (C_S)

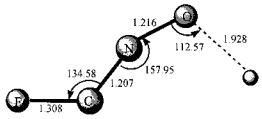

TSa_3P_{14} (C_S)

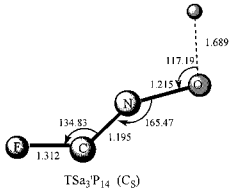

$TSa_3'P_{14}$ (C_S)

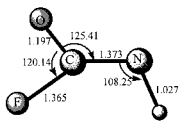

TSb_1b_1 (C_S)

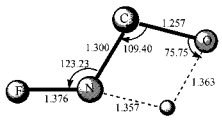

$TSb_4'b_5$ (C_S)

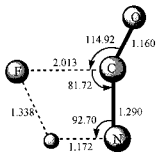

TSb_1P_1 (C_S)

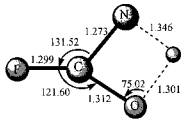

$TSsb_1b_2$ (C_S)

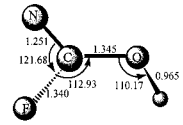

OCFN=182.85 HOCF=-93.64

TSb_2b_2' (C_1)

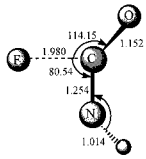

NCFO=172.83 HNCF=60.47

TSb_1P_2 (C_1)

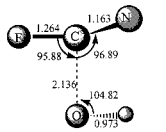

OCFN=-182.55 HOCF=-202.11

TSb_2P_4 (C_1)

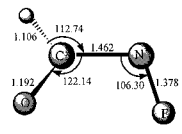

OCNF=86.02 HCNO=175.93

TSb_3b_3' (C_1)

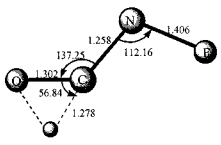

TSb_3b_4 (C_S)

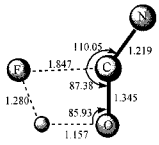

$TSb_2'P_1$ (C_S)

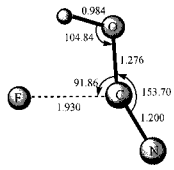

$TSb_2'P_5$ (C_S)

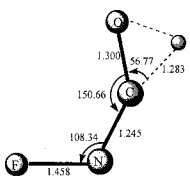

$TSb_2'b_4'$ (C_S)

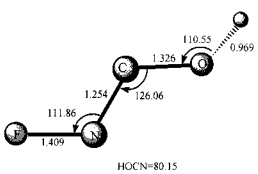

HOCN=80.15

TSb_4b_4' (C_1)

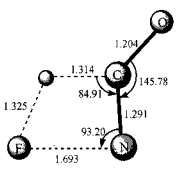

TSb_3P_1 (C_S)

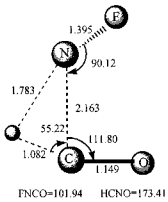

FNCO=101.94 HCNO=173.41

TSb_2P_3 (C_1)

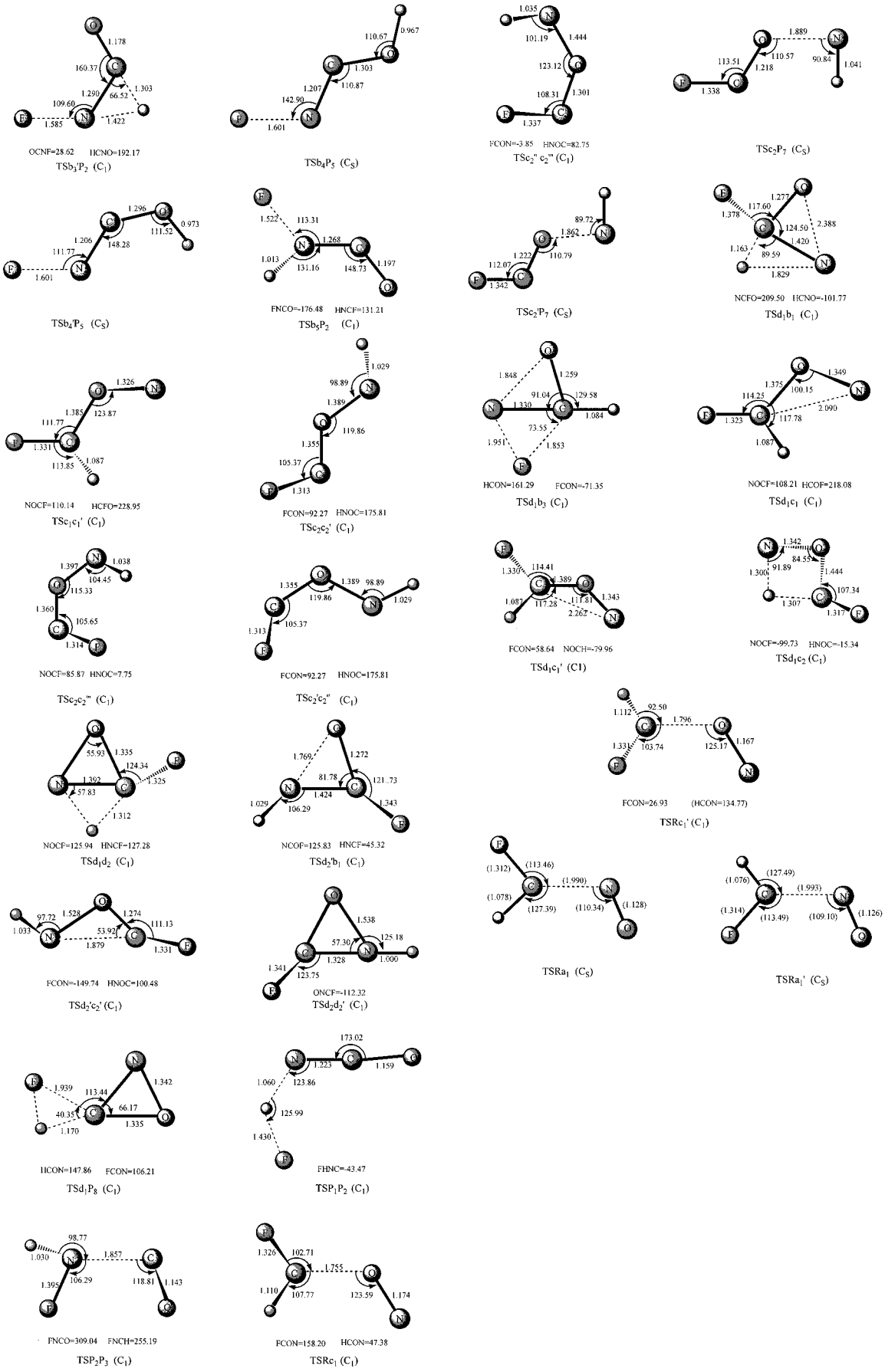

Figure 2. B3LYP/6-311G(d,p)-optimized geometries of all transition states. Bond distances are in angstroms and angles are in degrees. The HF/6-311G(d,p) values for **TSRa$_1$** and **TSRa$_1$′** are given in parentheses.

TABLE 3: Zero-Point Vibration Energies (hartree), Total Energies (TE) (hartree), and Relative Energies (RE) (kcal/mol) for All Transition States at the B3LYP/6-311G(d,p) Level and the QCISD(T)/6-311G(df,p)//B3LYP/6-311G(d,p) Level

species	ZPE	BTE	BRE	QTE	QRE
TSa$_1$a$_1$′	0.023552	−268.471517	−58.2	−267.948859	−47.2
TSa$_1$a$_3$	0.019203	−268.391319	−10.7	−267.876151	−4.4
TSa$_1$′a$_2$	0.017645	−268.370833	1.2	−267.853103	9.1
TSa$_2$a$_2$′	0.021999	−268.387753	−6.7	−267.871088	0.6
TSa$_2$a$_3$″	0.017686	−268.340857	20.1	−267.821692	28.9
TSa$_2$′a$_3$′	0.017933	−268.349852	14.6	−267.831628	22.8
TSa$_3$a$_3$′	0.023174	−268.436367	−36.4	−267.923721	−31.8
TSa$_3$″a$_3$‴	0.022835	−268.426587	−30.5	−267.913533	−25.5
TSa$_1$d$_1$	0.023184	−268.431340	−33.3	−267.917694	−27.9
TSa$_2$′d$_2$′	0.021517	−268.377658	−0.6	−267.861965	6.0
TSa$_1$P$_{14}$	0.018231[a]	−267.693601[a]	24.5[a]	−267.826222	26.4
TSa$_1$′P$_6$	0.018356	−268.395042	−13.5	−267.854562	8.7
TSa$_1$′P$_{12}$	0.025005[a]	−267.731292[a]	5.1[a]	−267.866069	5.6
TSa$_2$′P$_6$	0.036819	−268.342460	31.1	−267.817698	43.4
TSa$_3$P$_{14}$	0.014149	−268.342822	16.6	−267.831873	20.3
TSa$_3$′P$_4$	0.021029	−268.415075	−24.4	−267.897466	−16.6
TSa$_3$′P$_{14}$	0.014403	−268.339080	19.1	−267.819154	28.4
TSb$_1$b$_1$	0.023173	−268.535693	−98.8	−268.024213	−94.8
TSb$_1$b$_2$	0.020182	−268.463792	−55.5	−267.953481	−52.3
TSb$_2$b$_2$′	0.024150	−268.515141	−85.2	−268.004793	−82.0
TSb$_3$b$_3$′	0.022588	−268.451665	−46.4	−267.937510	−40.7
TSb$_3$b$_4$	0.017791	−268.372294	0.4	−267.852585	9.6
TSb$_3$′b$_4$′	0.017480	−268.369178	2.2	−267.847707	12.4
TSb$_4$b$_4$′	0.022767	−268.431057	−33.4	−267.914601	−26.2
TSb$_4$′b$_5$	0.018240	−268.362431	−6.9	−267.845909	14.0
TSb$_1$P$_1$	0.018976	−268.467014	−58.3	−267.937061	−42.7
TSb$_1$P$_2$	0.022482	−268.502862	−78.6	−267.970367	−61.4
TSb$_2$P$_4$	0.020523	−268.449148	−46.1	−267.936757	−41.6
TSb$_2$′P$_1$	0.018227	−268.455065	−51.3	−267.927840	−37.4
TSb$_2$′P$_5$	0.022015	−268.429511	−32.9	−267.891047	−11.9
TSb$_3$P$_1$	0.016699	−268.394407	−14.2	−267.865635	0.7
TSb$_3$P$_3$	0.018155	−268.354509	11.8	−267.826065	26.4
TSb$_3$′P$_2$	0.017844	−268.406505	−21.0	−267.879977	2.1
TSb$_4$P$_5$	0.021404	−268.427489	−31.9	−267.903772	−20.3
TSb$_4$′P$_5$	0.021112	−268.425017	−30.6	−267.901311	−18.9
TSb$_5$P$_2$	0.022293	−268.457841	−50.5	−267.929320	−35.8
TSc$_1$c$_1$′	0.021213	−268.380951	−2.9	−267.865115	3.8
TSc$_2$c$_2$′	0.021050	−268.398426	−14.0	−267.889484	−11.6
TSc$_2$c$_2$‴	0.020777	−268.377651	−1.1	−267.867706	1.9
TSc$_2$′c$_2$‴	0.021366	−268.383195	−4.2	−267.872320	−0.6
TSc$_2$″c$_2$‴	0.020791	−268.399859	−15.0	−267.889614	−11.8
TSc$_2$P$_7$	0.018345	−268.365781	4.8	−267.845457	14.4
TSc$_2$′P$_7$	0.018250	−268.366443	4.4	−267.845444	14.3
TSd$_1$b$_1$	0.018998	−268.398511	−15.3	−267.877816	−5.5
TSd$_1$b$_3$	0.021306	−268.373297	2.0	−267.849048	14.0
TSd$_1$c$_1$	0.021247	−268.389460	−8.2	−267.876632	−3.4
TSd$_1$c$_1$′	0.021213	−268.381942	−3.5	−267.868192	1.9
TSd$_1$c$_2$	0.018370	−268.361835	7.3	−267.857493	6.8
TSd$_1$d$_2$	0.018807	−268.352649	13.4	−267.846118	14.2
TSd$_2$′b$_1$	0.022528	−268.416841	−24.6	−267.908610	−22.6
TSd$_2$′c$_2$′	0.021664	−268.378887	−1.3	−267.867614	2.6
TSd$_2$d$_2$′	0.022229	−268.381092	−2.3	−267.870694	1.0
TSd$_1$P$_8$	0.017690	−268.359500	8.4	−267.839425	17.7
TSP$_1$P$_2$	0.019769	−268.501558	−79.5	−267.966693	−60.8
TSP$_2$P$_3$	0.021494	−268.443533	−42.0	−267.927698	−35.3
TSRc$_1$	0.019554	−268.367986	4.2	−267.847310	14.0
TSRc$_1$′	0.020111	−268.371518	2.3	−267.853968	8.0
TSRa$_1$				−267.873685	−5.6
TSRa$_1$′				−267.874988	−6.3

[a] The calculated results at the MP2/6-311G(d,p) level. [b] Since **TSRa$_1$** and **TSRa$_1$′** are obtained at the HF/6-311G(d,p) level, only the single-point QCISD(T)/6-311G(df,p) energies are given.

mol) exists to give the O-attack chainlike isomer H_2CON. At the B3LYP/6-311G(d,p) level, we cannot obtain the transition state linking **R** to the three-membered ring isomer **d$_1$**. Yet, we expect the formation of **d$_1$** to be a barrier-consumed process since significant C−N and C−O single bond formation and N−O multiple bond weakening are involved. As a result, only the end N-attack is a feasible way.

Starting from the CNO-chain isomer **a$_1$** or **a$_1$′**, various products may be obtained via successive isomerization and dissociation pathways. In the following parts, we will first

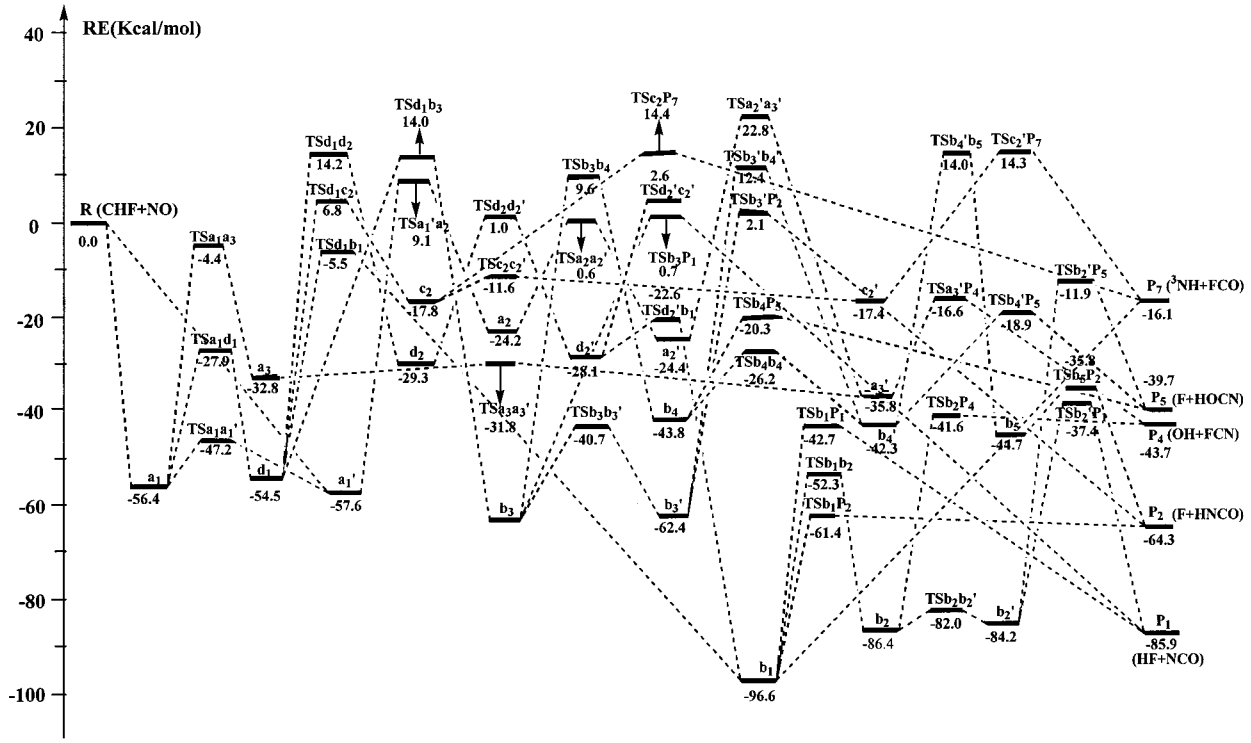

Figure 3. Potential energy surface of the favorable reaction channels for the ^{1}CHF + NO reaction at the QCISD(T)/6-311G(df,p)//B3LYP/-311G-(d,p) level.

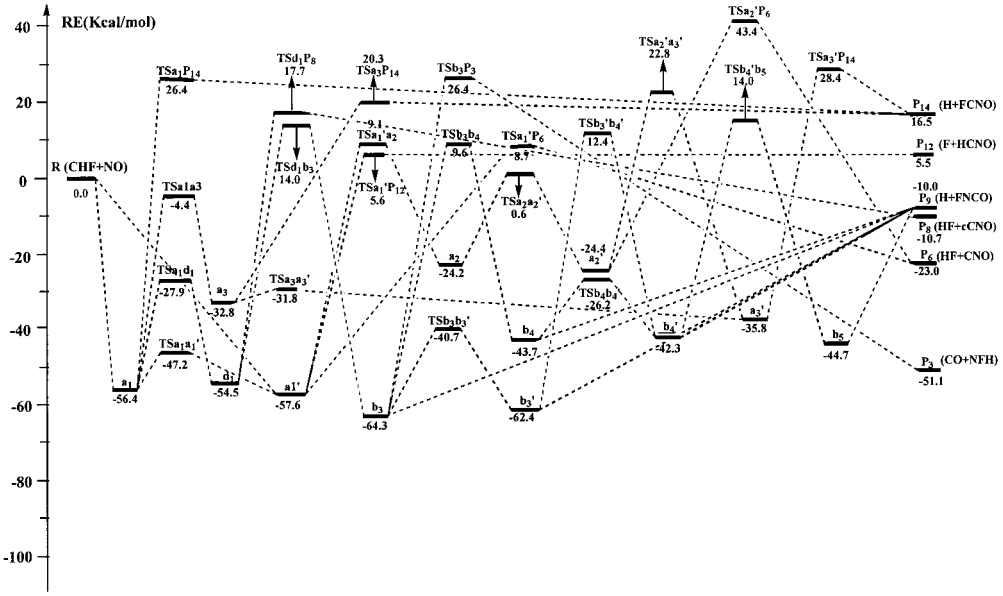

Figure 4. Potential energy surface of the unfavorable reaction channels for the ^{1}CHF + NO reaction at the QCISD(T)/6-311G(df,p)//B3LYP/-311G(d,p) level.

discuss the formation pathways of the five feasible products $\mathbf{P_1}$ HF + NCO, $\mathbf{P_2}$ F + HNCO, $\mathbf{P_4}$ OH + FCN, $\mathbf{P_5}$ F + HOCN, and $\mathbf{P_7}$ ^{3}NH + FCO.

3.2.1. $\mathbf{P_1}$ HF + NCO. $\mathbf{P_1}$ is the lowest-energy product. From Figure 3, we can find that only two pathways are energetically possible as

Path $\mathbf{P_1(I)}$ $\quad \mathbf{R} \rightarrow \mathbf{a_1}\,(\mathbf{a_1}') \rightarrow \mathbf{d_1} \rightarrow \mathbf{b_1} \rightarrow \mathbf{P_1}$ HF + NCO

Path $\mathbf{P_1(II)}$ $\quad \mathbf{R} \rightarrow \mathbf{a_1}\,(\mathbf{a_1}') \rightarrow \mathbf{d_1} \rightarrow \mathbf{b_1} \rightarrow \mathbf{b_2} \rightarrow \mathbf{b_2}' \rightarrow \mathbf{P_1}$ HF + NCO

For simplicity, the *cis*−*trans* isomerization process between $\mathbf{a_1}$ and $\mathbf{a_1}'$ is not shown in both pathways. The CNO-chain isomer $\mathbf{a_1}$ first takes a ring-closure to form the three-membered ring isomer $\mathbf{d_1}$ followed by a concerted H-shift to the N-atom and ring-open to give the lowest-lying NCO-chain isomer HNC(F)O $\mathbf{b_1}$. Isomer $\mathbf{b_1}$ may either undergo a direct HF-side extrusion to give $\mathbf{P_1}$ as in path $\mathbf{P_1(I)}$, or a 1,3-H-shift to give the second low-lying NCO-chain isomer NC(F)OH $\mathbf{b_2}$ followed by *cis*−*trans* isomerization to $\mathbf{b_2}'$ and subsequent HF-side extrusion of $\mathbf{b_2}'$ to give $\mathbf{P_1}$ as in Path $\mathbf{P_1(II)}$.

In path $\mathbf{P_1(II)}$, two high barriers are needed to overcome from $\mathbf{b_1}$ to $\mathbf{P_1}$, i.e., 44.3 and 46.8 kcal/mol for $\mathbf{b_1} \rightarrow \mathbf{b_2}$ and $\mathbf{b_2}' \rightarrow \mathbf{P_1}$ conversions, respectively. Yet in path $\mathbf{P_1(I)}$, only one high barrier 51.9 kcal/mol for $\mathbf{b_1} \rightarrow \mathbf{P_1}$ is needed. Moreover, $\mathbf{TSb_2'P_1}$

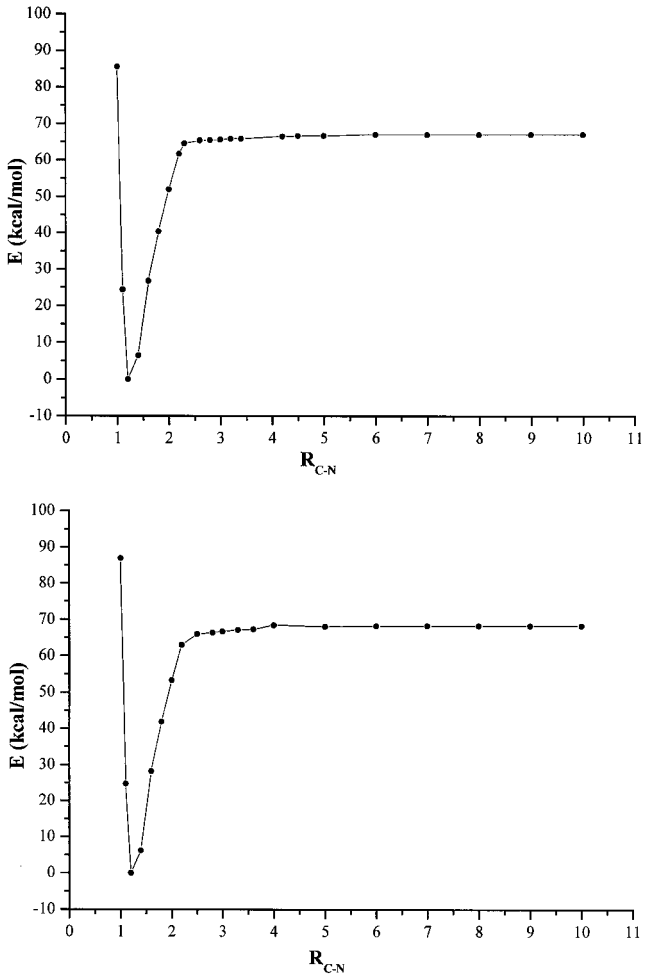

Figure 5. (a) Dissociation curve for HFCNO $\mathbf{a_1}$ at the B3LYP/6-311G-(d,p) level. (b) Dissociation curve for HFCNO $\mathbf{a_1}'$ at the B3LYP/6-311G(d,p) level.

is 5.3 kcal/mol higher in energy than $\mathbf{TSb_1P_1}$. Then, we expect that path $\mathbf{P_1(I)}$ may be more competitive than path $\mathbf{P_1(II)}$.

3.2.2. $\mathbf{P_2}$ F + HNCO. For the second low-lying product $\mathbf{P_2}$ F + HNCO, only one pathway is feasible via the channel:

$$\text{Path } \mathbf{P_2(I)}\ \mathbf{R \rightarrow a_1\ (a_1') \rightarrow d_1 \rightarrow b_1 \rightarrow P_2\ F + HNCO}$$

The formation of $\mathbf{b_1}$ is the same as that in path $\mathbf{P_1(I)}$ and path $\mathbf{P_1(II)}$. Isomer $\mathbf{b_2}$ can directly dissociate to form $\mathbf{P_2}$ F + HNCO via $\mathbf{TSb_1P_2}$. The dissociation barrier 35.2 kcal/mol is very close to the dissociation limit 32.3 kcal/mol from $\mathbf{b_1}$ to $\mathbf{P_2}$.

3.2.3. $\mathbf{P_4}$ OH + FCN. There are two feasible pathways to form $\mathbf{P_4}$ OH + FCN. They can be written as follows:

$$\text{Path } \mathbf{P_4(I)}\quad \mathbf{R \rightarrow a_1\ (a_1') \rightarrow a_3 \rightarrow a_3' \rightarrow P_4}\ \text{OH + FCN}$$

$$\text{Path } \mathbf{P_4(II)}\quad \mathbf{R \rightarrow a_1\ (a_1') \rightarrow d_1 \rightarrow b_1 \rightarrow b_2 \rightarrow P_4}\ \text{OH + FCN}$$

In path $\mathbf{P_4(I)}$, the initially formed isomer $\mathbf{a_1}$ requires a 1,3-H-shift to form $\mathbf{a_3}$. The *cis*−*trans* isomerization of $\mathbf{a_3}$ then easily takes place followed by direct N−O bond dissociation leading to $\mathbf{P_4}$. Path $\mathbf{P_4(II)}$ is very similar to path $\mathbf{P_1(II)}$ except that $\mathbf{b_2}$ directly dissociates the C−O bond to form $\mathbf{P_4}$ instead of *cis*−*trans* conversion and side HF extrusion to form $\mathbf{P_1}$.

Four high barriers have to be climbed in path $\mathbf{P_4(II)}$, which are 28.5 ($\mathbf{a_1 \rightarrow d_1}$), 49.0 ($\mathbf{d_1 \rightarrow b_1}$), 44.3 ($\mathbf{b_1 \rightarrow b_2}$), and 44.8 ($\mathbf{b_2 \rightarrow P_4}$) kcal/mol. In path $\mathbf{P_4(I)}$, only two high barriers 52.0 ($\mathbf{a_1 \rightarrow a_3}$) and 19.2 ($\mathbf{a_3' \rightarrow P_4}$) kcal/mol are needed. Though the highest transition state $\mathbf{TSd_1b_1}$ (−5.5 kcal/mol) in path $\mathbf{P_4(II)}$ is 1.1 kcal/mol lower than $\mathbf{TSa_1a_3}$ in path $\mathbf{P_4(I)}$, we still expect that path $\mathbf{P_4(I)}$ may be more competitive than path $\mathbf{P_4(II)}$. In fact, as will be shown later, path $\mathbf{P_4(II)}$ is much less competitive than path $\mathbf{P_2(I)}$.

3.2.4. $\mathbf{P_5}$ F + HOCN and $\mathbf{P_7}$ ^{3}NH + FCO. Only one feasible pathway is associated with formation of either $\mathbf{P_5}$ F + HOCN or $\mathbf{P_7}$ ^{3}NH + FCO, which is via the direct dissociation of $\mathbf{b_2}'$ and $\mathbf{b_1}$, respectively. The two pathways can be written as

$$\text{Path } \mathbf{P_5(I)}\quad \mathbf{R \rightarrow a_1\ (a_1') \rightarrow d_1 \rightarrow b_1 \rightarrow b_2 \rightarrow b_2' \rightarrow P_5}\ \text{F + HOCN}$$

$$\text{Path } \mathbf{P_7(I)}\ \mathbf{R \rightarrow a_1\ (a_1') \rightarrow d_1 \rightarrow b_1 \rightarrow P_7}\ ^3\text{NH + FCO}$$

Path $\mathbf{P_5(I)}$ is very similar to path $\mathbf{P_1(II)}$. The difference lies in the last dissociation step, i.e., in path $\mathbf{P_5(I)}$, the NCO-chain isomer $\mathbf{b_2}'$ directly dissociates to $\mathbf{P_5}$ via the C−F rupture, while in path $\mathbf{P_1(II)}$, $\mathbf{b_2}'$ leads to $\mathbf{P_1}$ via a side HF-extrusion process. The last step of path $\mathbf{P_7(I)}$ results in a direct N−C cleavage of $\mathbf{b_1}$ to form $\mathbf{P_7}$ instead of the product ^{1}NH + FCO. We cannot locate any dissociation transition state $\mathbf{TSb_1P_7}$.

3.2.5. $\mathbf{P_3}$ CO + NFH, $\mathbf{P_6}$ HF + CNO, $\mathbf{P_8}$ HF + c-CNO, and $\mathbf{P_9}$ H + FNCO. The products $\mathbf{P_3}$, $\mathbf{P_6}$, $\mathbf{P_8}$, and $\mathbf{P_9}$ are all thermodynamically possible products that lie 51.1, 23.0, 10.7, and 10.0 kcal/mol below the reactant **R**, respectively. Yet, they are all kinetically unfeasible due to the involved high-energy transition states. The formation of $\mathbf{P_3}$ and $\mathbf{P_9}$ must proceed via the NCO-chain isomer $\mathbf{b_3}$. Since $\mathbf{b_3}$ can only be formed from the three-membered ring isomer $\mathbf{d_1}$ via the high-energy $\mathbf{TSd_1b_3}$, that is 14.0 kcal/mol above **R**, observation of $\mathbf{P_3}$ and $\mathbf{P_9}$ is kinetically prohibited. $\mathbf{P_6}$ can be obtained either via the end HF-extrusion of the CNO-chain isomer $\mathbf{a_1}'$ or via the side HF-extrusion of another CNO-chain isomer $\mathbf{a_2}'$. $\mathbf{P_8}$ can be formed from the three-membered ring isomer $\mathbf{d_1}$. Since the transition states $\mathbf{TSa_1'P_6}$, $\mathbf{TSa_2'P_6}$ and $\mathbf{TSd_1P_8}$ are 8.7, 43.4, and 17.7 kcal/mol higher than **R**, formation of $\mathbf{P_6}$ and $\mathbf{P_8}$ is less likely.

3.3. Mechanism of the ^{1}CHF + NO Reaction. Let us discuss the possible mechanism of the ^{1}CHF + NO reaction. For easier discussion, we list the feasible pathways for the products $\mathbf{P_1}$, $\mathbf{P_2}$, $\mathbf{P_4}$, $\mathbf{P_5}$, and $\mathbf{P_7}$ again:

$$\text{Path } \mathbf{P_1(I)}\quad \mathbf{R \rightarrow a_1\ (a_1') \rightarrow d_1 \rightarrow b_1 \rightarrow P_1}\ \text{HF + NCO}$$

$$\text{Path } \mathbf{P_1(II)}\quad \mathbf{R \rightarrow a_1\ (a_1') \rightarrow d_1 \rightarrow b_1 \rightarrow b_2 \rightarrow b_2' \rightarrow P_1}\ \text{HF + NCO}$$

$$\text{Path } \mathbf{P_2(I)}\quad \mathbf{R \rightarrow a_1\ (a_1') \rightarrow d_1 \rightarrow b_1 \rightarrow P_2}\ \text{F + HNCO}$$

$$\text{Path } \mathbf{P_4(I)}\quad \mathbf{R \rightarrow a_1\ (a_1') \rightarrow a_3 \rightarrow a_3' \rightarrow P_4}\ \text{OH + FCN}$$

$$\text{Path } \mathbf{P_4(II)}\quad \mathbf{R \rightarrow a_1\ (a_1') \rightarrow d_1 \rightarrow b_1 \rightarrow b_2 \rightarrow P_4}\ \text{OH + FCN}$$

$$\text{Path } \mathbf{P_5(I)}\quad \mathbf{R \rightarrow a_1\ (a_1') \rightarrow d_1 \rightarrow b_1 \rightarrow b_2 \rightarrow b_2' \rightarrow P_5}\ \text{F + HOCN}$$

$$\text{Path } \mathbf{P_7(I)}\quad \mathbf{R \rightarrow a_1\ (a_1') \rightarrow d_1 \rightarrow b_1 \rightarrow P_7}\ ^3\text{NH + FCO}$$

We can easily find that except for path $\mathbf{P_4(I)}$, all the pathways involve the low-lying three-membered ring isomer c-C(H_2)NO $\mathbf{d_1}$ and the lowest-energy NCO-chain isomer $\mathbf{b_1}$. We first compare these c-C(H_2)NO $\mathbf{d_1}$ and OC(F)NH $\mathbf{b_1}$-involved pathways. Starting from OC(F)NH $\mathbf{b_1}$, the direct dissociation to $\mathbf{P_7}$ is the least feasible due to the high-energy of $\mathbf{P_7}$ (−16.1).

Also, due to the rather high-energy of $\mathbf{TSb_2'P_5}$ (−11.9), formation of $\mathbf{P_5}$ is quite uncompetitive. Furthermore, the direct dissociation transition state $\mathbf{TSb_1P_2}$ (−61.4) in path $\mathbf{P_2(I)}$ is significantly lower than $\mathbf{TSb_1b_2}$ (−52.3), $\mathbf{TSb_1P_1}$ (−42.7), $\mathbf{TSb_2P_4}$ (−41.6), and $\mathbf{TSb_2'P_1}$ (−37.4) in path $\mathbf{P_1(I)}$, path $\mathbf{P_1(II)}$, and path $\mathbf{P_4(II)}$, the pathway path $\mathbf{P_2(I)}$ should be much more competitive than path $\mathbf{P_1(I)}$, path $\mathbf{P_1(II)}$, and path $\mathbf{P_4(II)}$. Thus, path $\mathbf{P_2(I)}$ is the most feasible pathway that is associated with c-C(HF)NO $\mathbf{d_1}$ and OC(F)NH $\mathbf{b_1}$ on the basis of energetic considerations. Simply from the energies, it is somewhat difficult to compare which is the most favorable among path $\mathbf{P_1(I)}$, path $\mathbf{P_1(II)}$, and path $\mathbf{P_4(II)}$ since the involved transition states $\mathbf{TSb_1P_1}$ (−42.7), $\mathbf{TSb_2P_4}$ (−41.6), and $\mathbf{TSb_2'P_1}$ (−37.4) do not differ so much in their energetics.

Path $\mathbf{P_4(I)}$ proceeds simply via the CNO-chain isomers HFCNO $\mathbf{a_1}$, FCNOH $\mathbf{a_3}$ and $\mathbf{a_3'}$. It seems difficult to compare the feasibility between path $\mathbf{P_4(I)}$ and path $\mathbf{P_2(I)}$ without detailed dynamical calculations. The highest transition state $\mathbf{TSd_1b_1}$ (−5.5) in path $\mathbf{P_2(I)}$ is 1.1 kcal/mol lower than $\mathbf{TSa_1a_3}$ (−4.4) in path $\mathbf{P_4(I)}$. On the other hand, more high barriers are involved in path $\mathbf{P_2(I)}$ than in path $\mathbf{P_4(I)}$. Then, we tentatively expect that both pathways may have comparable contribution to the reaction ^{1}CHF + NO, i.e., among the final product distributions, $\mathbf{P_2}$ F + HNCO and $\mathbf{P_4}$ OH + NCO may have comparable branching ratios.

To deeply understand the mechanism of the title reaction, we perform the simple multichannel Rice−Ramsperger−Kassel−Marcus (RRKM) calculations[29,30] for the major products $\mathbf{P_1}$ HF + OCN, $\mathbf{P_2}$ F + HNCO, and $\mathbf{P_4}$ OH + FCN. We consider the following reaction pathways:

$$\mathrm{CHF} + \mathrm{NO} \underset{k_{11}}{\overset{k_a}{\rightleftharpoons}} \mathrm{HFCNO^*}\ (\mathbf{a_1}) \underset{k_{21}}{\overset{k_{12}}{\rightleftharpoons}} \mathrm{FCNOH^*}\ (\mathbf{a_3}) \xrightarrow{k_{22}} \mathbf{P_4}\ \mathrm{OH} + \mathrm{FCN}$$

$$\xrightarrow{k_{2w}} \mathrm{FCNOH}$$

$$\underset{k_{31}}{\overset{k_{13}}{\rightleftharpoons}} \text{c-C(HF)NO*}(\mathbf{d_1}) \underset{k_{41}}{\overset{k_{32}}{\rightleftharpoons}} \mathrm{HNC(F)O^*}\ (\mathbf{b_1}) \xrightarrow{k_{42}} \mathbf{P_1}\ \mathrm{HF} + \mathrm{OCN}$$

$$\xrightarrow{k_{1w}} \mathrm{HFCNO} \qquad \xrightarrow{k_{3w}} \text{c-HF-CNO} \qquad \xrightarrow{k_{43}} \mathbf{P_2}\ \mathrm{F} + \mathrm{HNCO}$$

$$\underset{k_{51}}{\overset{k_{44}}{\rightleftharpoons}} \mathrm{NC(F)OH^*}\ (\mathbf{b_2}) \xrightarrow{k_{52}} \mathbf{P_1}\ \mathrm{HF} + \mathrm{OCN}$$

$$\xrightarrow{k_{4w}} \mathrm{HNC(F)O} \qquad \xrightarrow{k_{53}} \mathbf{P_4}\ \mathrm{OH} + \mathrm{FCN}$$

$$\xrightarrow{k_{5w}} \mathrm{NC(F)OH}$$

where "*" represents the vibrational excitation of the intermediates. To compare the predicted values with the experimental data, we choose the fixed pressure of 4.5 Torr of Ar. Using the vibrational frequencies and partitional functions of $\mathbf{TSRa_1}$ obtained at the HF/6-311G(d,p), we find that when the entrance barrier is set to 0.2 kcal/mol, the total theoretical rate constant 7.2×10^{-12} cm^3 molecule^{-1} s^{-1} can well match the experimental value $(7.0 \pm 0.4) \times 10^{-12}$ cm^3 molecule^{-1} s^{-1}.[13] The calculated branching ratios of $\mathbf{P_1}$ HF + NCO, $\mathbf{P_2}$ F + HNCO, and $\mathbf{P_4}$ OH + FCN are depicted in Figure 6. We can see that within the temperature range 200−2000 K, $\mathbf{P_1}$ HF + NCO occupies a minor branching ratio of less than 15%, while $\mathbf{P_2}$ F + HNCO and $\mathbf{P_4}$ OH + FCN have predominant abundance. At moderate and high temperatures, $\mathbf{P_4}$ OH + FCN has a larger branching ratio than $\mathbf{P_2}$ F + HNCO, whereas at temperatures lower than 320 K, the branching ratio of $\mathbf{P_4}$ gets somewhat smaller than that of $\mathbf{P_2}$.

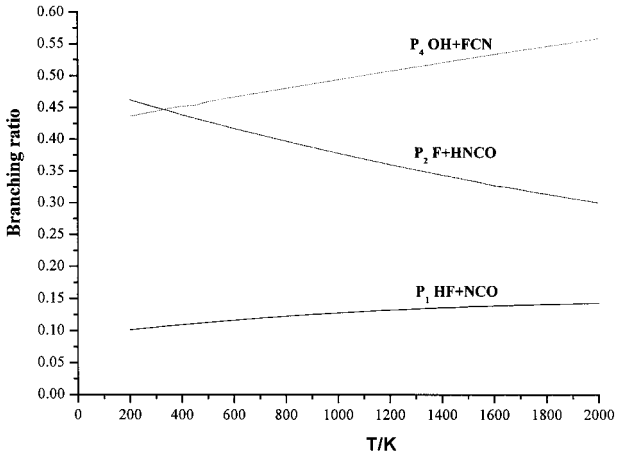

Figure 6. Branching ratios for the products $\mathbf{P_1}$ HF + NCO, $\mathbf{P_2}$ F + HNCO, and $\mathbf{P_4}$ OH + FCN with a pressure of 4.5 Torr Ar.

As a result, reflected in the final product distributions, we predict that (1) a total of five kinds of products $\mathbf{P_1}$ HF + NCO, $\mathbf{P_2}$ F + HNCO, $\mathbf{P_4}$ OH + NCO, $\mathbf{P_5}$ F + HOCN, and $\mathbf{P_7}$ ^{3}NH + FCO are thermodynamically and kinetically feasible; (2) $\mathbf{P_2}$ F + HNCO and $\mathbf{P_4}$ OH + NCO may be the most feasible products with comparable branching ratios, and at higher temperatures, $\mathbf{P_4}$ may have more abundance than $\mathbf{P_2}$; (3) $\mathbf{P_1}$ may be much less feasible than $\mathbf{P_2}$ and $\mathbf{P_4}$; and (4) $\mathbf{P_5}$ and $\mathbf{P_7}$ are the least feasible products with almost negligible yields.

3.4. Comparison with the $^3CH_2$ + NO Reaction. The analogous reaction $^3CH_2$ + NO has been extensively studied by both experimentalists[16,18−22] and theoreticians.[17,23−25] We mainly compare our calculated CHFNO potential energy surface with the CH_2NO one obtained by Shapley and Bacskay.[24,25] Their obtained mechanism may be summarized as follows:

Path 1 $^3CH_2 + NO \rightarrow H_2CNO \rightarrow H + HCNO$

Path 2 $^3CH_2 + NO \rightarrow H_2CNO \rightarrow \text{c-C}(H_2)NO \rightarrow OC(H_2)N \rightarrow HNC(H)O \rightarrow H + HNCO$

Path 3 $^3CH_2 + NO \rightarrow H_2CNO \rightarrow \text{c-C}(H_2)NO \rightarrow OC(H_2)N \rightarrow HNC(H)O \rightarrow H_2NCO \rightarrow NH_2 + CO$

Path 4 $^3CH_2 + NO \rightarrow H_2CNO \rightarrow \text{c-C}(H_2)NO \rightarrow OC(H_2)N \rightarrow HOC(H)N \rightarrow OH + HCN$

Path 5 $^3CH_2 + NO \rightarrow H_2CNO \rightarrow \text{c-C}(H_2)NO \rightarrow OC(H_2)N \rightarrow HOC(H)N \rightarrow H + HOCN$

They concluded that all five products should be observable, among which H + HCNO is the most abundant, and the other four may have comparable yields. Their prediction is somewhat different from the experimental observation that H + HCNO occupies 84% and OH + HCN 15%. To distinguish from our pathways, those calculated by Shapley and Bacskay are labeled in italics.

Nearly all the isomerization and dissociation pathways are considered except those products with higher energies than the reactants. The most significant difference is that there is a

kinetically unstable intermediate OCH_2N between the three-membered ring isomer c-C(H_2)NO and the NCO-chain isomer HNCHO for the $^3CH_2$ + NO reaction, whereas such an intermediate does not exist for the ^{1}CHF + NO reaction. Another important energetic discrepancy is that for the $^3CH_2$ + NO reaction, the lowest-lying isomer is the NCO-chain isomer H_2NCO, whereas for the ^{1}CHF + NO reaction, the NCO-chain isomer HNC(F)O **b$_1$** has the lowest energy.

Generally, our calculated potential energy surface for the ^{1}CHF + NO reaction is quite parallel to that of the $^3CH_2$ + NO reaction. The discrepancy is just quantitative. For example, the direct C−F and C−H bond cleavage transition states of the initially formed CNO-chain isomer HFCNO **a$_1$** (**a$_1$′**), i.e., **TSa$_1$P$_{14}$** and **TSa$_1$′P$_{12}$** leading to **P$_{14}$** H + FCNO and **P$_{12}$** F + HCNO, respectively, are 26.4 and 5.6 kcal/mol higher than **R** ^{1}CHF + NO. In fact, **P$_{14}$** and **P$_{12}$** lie 16.5 and 5.5 kcal/mol above **R** ^{1}CHF + NO. Yet for the $^3CH_2$ + NO reaction, the C−H bond cleavage limit in *Path P$_1$*, i.e., H + HCNO, is 22.8 kcal/mol below the reactants, and is even 4.7 kcal/mol lower than the rate-determining transition state from the NCO three-membered ring isomer c-C(H_2)NO to the NCO-chain isomer HNC(H)O in *Path P$_2$*, *P$_3$*, *P$_4$*, and *P$_5$*. On the other hand, the 1,3-H-shift transition state from H_2CNO to HCNOH is 3.8 kcal/mol higher than the reactants $^3CH_2$ + NO, whereas for the ^{1}CHF + NO reaction, such a transition state **TSa$_1$a$_3$** in path **P$_4$(I)** is 4.4 kcal/mol lower than the reactants and is just 1.1 kcal/mol higher than **TSd$_1$b$_1$** linking the three-membered ring isomer c-C(HF)NO **d$_1$** to the NCO-chain isomer HNC(F)O (**b$_1$**). As a result, for the ^{1}CHF + NO reaction, the formation of **P$_4$** OH + FCN via path **P$_4$(I)** is very feasible and may even be comparable with that of **P$_2$** F + HNCO via path **P$_2$(I)**.

3.5. Experimental Implication for the ^{1}CHF + NO Reaction. Now we turn to the comparison between our calculated mechanism and the available experimental results for the ^{1}CHF + NO reaction. Two papers by Hancock's group[13,14] have reported the FTIR investigation on this reaction. Only two reaction channels were identified, namely, **P$_1$** HF + NCO and **P$_2$** F + HNCO with the corresponding branching ratio 6:4.[14] Their results are in marked difference from our theoretical prediction that five products **P$_1$** HF + NCO, **P$_2$** F + HNCO, **P$_4$** OH + FCN, **P$_5$** F + HOCN, and **P$_7$** ^{3}NH + FCO are energetically accessible, among which **P$_2$** and **P$_4$** may have predominant abundance with comparable yields and **P$_1$** is much less (at 295 K, the branching ratios of **P$_1$**, **P$_2$**, and **P$_4$** are 0.11, 0.45, and 0.44, respectively), while **P$_5$** and **P$_7$** have almost negligible branching ratios. We locate a secondary transition state **TSP$_1$P$_2$** that lies 3.5 kcal/mol above **P$_2$**. Provided that the F-atom and HNCO molecule in **P$_2$** do not separate, the large exothermicity 64.3 kcal/mol released from **R** to **P$_2$** is surely enough to promote such secondary H-abstraction. However, the small addition barrier 2.9 kcal/mol may also competitively drive F and HNCO to form **b$_1$**. That is, even the secondary reaction cannot account for the experimentally observed predominance of **P$_1$** HF + NCO. Since we have made a nearly complete search on the potential energy surface of ^{1}CHF + NO compared to that of the analogous $^3CH_2$ + NO reaction and the two reactions show quite parallel features despite some energetic discrepancies, we feel that further experimental investigation is desirable to clarify the mechanism of the ^{1}CHF + NO reaction.

4. Conclusions

A detailed doublet potential energy surface of the ^{1}CHF + NO reaction system is carried out at the B3LYP and QCISD(T) (single-point) levels. The main calculated results can be summarized as follows:

(1) Five dissociation products **P$_1$** HF + NCO, **P$_2$** F + HNCO, **P$_4$** OH + FCN, **P$_5$** F + HOCN, and **P$_7$** ^{3}NH + FCO are both thermodynamically and kinetically feasible. Among the five dissociation products, **P$_2$** and **P$_4$** may be the most abundant products with comparable quantities, whereas **P$_1$** is much less competitive followed by the least feasible **P$_5$** and **P$_7$**.

(2) Our calculated potential energy surface of ^{1}CHF + NO reaction is compared with that of the analogous $^3CH_2$ + NO reaction. Despite the energetic differences, both potential energy surfaces are very alike. Our results are quite different from previous experimental observation that only two dissociation products **P$_1$** and **P$_2$** are identified with the branching ratio being 6:4. Therefore, future experimental reinvestigations are desirable to clarify the mechanism of the title reaction.

Acknowledgment. This work is supported by the National Natural Science Foundation of China (No. 29892168, 20073014). We are very thankful for the referees' invaluable comments.

Supporting Information Available: Figure 7 show the B3LYP/6-311G(d,p)-optimized geometries of reactants and products. Bond distances are in angstroms and angles are in degrees. This material is available free of charge via the Internet at http://pubs.acs.org.

References and Notes

(1) *Halon Replacements*: Miziolek, A. W., Tsang, W., Eds.; ACS Symposium Series 611; American Chemical Society: Washington, DC, 1995.

(2) Brownsword, R. A.; Hancock, G.; Heard, D. E. *J. Chem. Soc., Faraday Trans*. **1991**, *87*, 2283.

(3) Cookson, J. L.; Hancock, G.; Mckendrick, K. G. *Ber. Bunsen-Ges., Phys. Chem*. **1985**, *89*, 335.

(4) Hancock, G.; Ketley. G. W.; MacRobert, A. J. *J. Phys. Chem*. **1984**, *88*, 2104.

(5) Herron, J. T. *J. Phys. Chem. Ref. Data* **1988**, *17*, 967.

(6) Tsai, C.; McFadden, D. L. *J. Phys. Chem*. **1990**, *94*, 3298.

(7) Zárate, A. O.; Martinez, R.; Rayo, M. N. S.; Castano, F.; Hancock, G. *J. Chem. Soc., Faraday Trans*. **1992**, *88*, 535.

(8) Miller, J. A.; Bowman, C. T. *Prog. Enery Combust. Sci*. **1989**, *15*, 287 and references therein.

(9) Wendt, J. O. L.; Sternling, C. V.; Matovich, M. A. In *14th symposium (International) on Combustion*; The Combustion Institute: Pittsburgh, PA, 1973; p 897.

(10) Myerson, A. L. In *15th Symposium (international) on Combustion*; The Combustion Institute: Pittsburgh, PA, 1975; p 1085

(11) Song, Y. H.; Blair, D. W.; Siminski, V. J.; Bartok, W. In *18th Symposium (International) on Combustion*; The Combustion Institute: Pittsburgh, PA, 1981; p 53.

(12) Chen, S. L.; McCarthy, J. M.; Clark, W. D.; Heap, M. P.; Seeker, W. R.; Pershing, D. W. In *21st Symposium (International) on Combuation*; The Combustion Institute: Pittsburgh, PA 1986; p 1159.

(13) Hancock, G.; Ketley, G. W. *J. Chem. Soc., Faraday Trans*. **1982**, *78*, 1283.

(14) Browsword, R. A.; Hancock, G.; Oum, K. W. *J. Phys. Chem*. **1996**, *100*, 4840.

(15) Melius, C. F. Private communication (1990).

(16) Grussdorf, F.; Temps, F.; Wagner, H. G. *Ber. Bunsen-Ges. Phys. Chem*. **1997**, *101*, 134.

(17) Roggenbuck, J.; Temps, F. *Chem. Phys. Lett*. **1998**, *285*, 422.

(18) Laufer, A. H.; Bass, A. M. *J. Phys. Chem*. **1974**, *78*, 1344.

(19) Vinckier, C.; Debruyn, W. *J. Phys. Chem*. **1979**, *83*, 2057.

(20) Seidler, V.; Temps, F.; Wagner, H. Gg.; Wolf, M. *J. Phys. Chem*. **1989**, *93*, 1070.

(21) Atakan, B.; Kocis, D.; Wolfrum, J.; Nelson, P. In *24th Symposium (International) on Combustion*; The Combustion Institute: Pittsburgh, PA, 1992; p 691.

(22) Bauerle, S.; Klatt, M.; Wagner, H. Gg. *Ber. Bunsen-Ges. Phys. Chem*. **1995**, *99*, 97.

(23) Shapley, W. A.; Bacskay, G. B. *Theor. Chem. Acc*. **1998**, *100*, 212.

(24) Shapley, W. A.; Bacskay, G. B. *J. Phys. Chem. A* **1999**, *103*, 4505.

(25) Shapley, W. A.; Bacskay, G. B. *J. Phys. Chem. A* **1999**, *103*, 4514.

(26) Frisch, M. J.; Trucks, G. W.; Schlegel, H. B.; Scuseria, G. E.; Robb, M. A.; Cheeseman, J. R.; Zakrzewski, V. G.; Montgomery, J. A., Jr.; Stratmann, R. E.; Burant, J. C.; Dapprich, S.; Millam, J. M.; Daniels, A.

D.; Kudin, K. N.; Strain, M. C.; Farkas, O.; Tomasi, J.; Barone, V.; Cossi, M.; Cammi, R.; Mennucci, B.; Pomelli, C.; Adamo, C.; Clifford, S.; Ochterski, J.; Petersson, G. A.; Ayala, P. Y.; Cui, Q.; Morokuma, K.; Malick, D. K.; Rabuck, A. D.; Raghavachari, K.; Foresman, J. B.; Cioslowski, J.; Ortiz, J. V.; Stefanov, B. B.; Liu, G.; Liashenko, A.; Piskorz, P.; Komaromi, I.; Gomperts, R.; Martin, R. L.; Fox, D. J.; Keith, T.; Al-Laham, M. A.; Peng, C. Y.; Nanayakkara, A.; Gonzalez, C.; Challacombe, M.; Gill, P. M. W.; Johnson, B.; Chen, W.; Wong, M. W.; Andres, J. L.; Gonzalez, C.; Head-Gordon, M.; Replogle, E. S.; Pople, J. A. *Gaussian98W*, Revision A.7; Gaussian, Inc., Pittsburgh, PA, 1998.

(27) (a) Born, M.; Ingemann, S.; Nibbering, N. M. M. *J. Am. Chem. Soc.* **1994**, *116*, 7210. (b) Sloan, J. J.; Watson, D. G.; Wright, J. S. *Chem. Phys.* **1979**, *43*, 1. (c) Sana, M.; Leroy, G. Peeter, D.; Younang, E. *J. Mol. Struct.* **1987**, *151*, 325. (d) Okabe, H. *Photochemistry of small molecules*: Wiley-Interscience: New York, 1978.

(28) Sloan, J. J.; Watson, D. G.; Wright, J. S. *Chem. Phys*. **1981**, *63*, 283.

(29) Diau, E. W. G.; Lin, M. C.; Melius, C. F. *J. Chem. Phys*. **1994**, *101*, 3923.

(30) Berman, M. R.; Lin, M. C. *J. Phys. Chem*. **1983**, *87*, 3933.